Efficient polymer solar cells based on the synergy effect of a novel non-conjugated small-molecule electrolyte and polar solvent†

Zhiyang Liu,[ab] Xinhua Ouyang,[a] Ruixiang Peng,[a] Yongqi Bai,[a] Dongbo Mi,[a] Weigang Jiang,[ab] Antonio Facchetti[c] and Ziyi Ge*[a]

A novel non-conjugated small-molecule electrolyte was invented as a cathode interlayer in PTB7:$PC_{71}BM$-based polymer solar cells (PSCs). We discovered a significant synergy effect for improving the device efficiency between methanol treatment and the interlayer. The methanol treatment mainly contributed to the open-circuit voltage, while the interlayer primarily enhanced the short-circuit current and fill factor. Under the effective synergy effect, power conversion efficiencies (PCEs) of PTB7:$PC_{71}BM$-based PSCs were largely improved from 3.89% to 9.79% for conventional PSCs and from 7.34% to 9.10% for inverted PSCs. Our findings create a new path of interfacial modification for highly efficient PSCs.

Introduction

Polymer solar cells with a bulk heterojunction (BHJ) structure have been a promising photovoltaic technology for renewable energies, owing to their light weight, mechanical flexibility, facile fabrication as well as their improving power conversion efficiencies (PCEs).[1] Recently, the PCEs of single-junction PSCs composed of π-conjugated polymers as the electron donors and fullerene derivatives as the electron acceptors have exceeded 10%.[2–4] PSCs are composed of multiple layers, where charge transport at each interface is critical for enhancing the efficiency. Therefore, interfacial engineering plays a key role in optimizing the charge extraction and recombination, contact resistance, electronic energy levels and optical absorption.[5–9] Numerous important efforts have addressed OPV interfacial modification, including the use of interlayers,[10] polar solvent processing,[11] surface plasmonic resonance[12] and nano-imprinting.[13] PSCs based on a metallic salt interlayer, such as LiF,[10a,b] have also been explored and usually need to be prepared by vacuum deposition, which limits their application in low-cost and large-area fabrication. Water/alcohol-soluble conjugated polyelectrolytes (CPEs)[14] and conjugated small-molecule organic interlayers[15] have also been successfully developed to improve the device performance, and have advantages such as orthogonal solubility to solvents used for the active layer, and eco-friendly large-area device fabrication processes.[16] However, those conjugated interfacial materials usually contain complicated π-conjugated moieties, demanding a difficult synthesis which may affect costs at a large scale. Hence, interfacial materials with simple structures, especially non-conjugated small-molecule electrolytes, are considered to be more promising candidates in the fabrication of low-cost and large-area PSCs.[17]

Non-conjugated polymers, such as polyethylenimide ethoxylated (PEIE),[8] poly(ethylene oxide) (PEO),[18] and poly (sulfobetaine methacrylate) (PSBMA),[19] can reduce the work function (WF) of electrodes due to their dipole moment. Therefore, we reasonably think that similar non-conjugated small-molecule organic electrolytes can also tune the electrode WF and affect the charge transport at the interface. Moreover, small-organic electrolytes have uncertain structures and molecular weights, which can address the disadvantages of metallic salts and conjugated interfacial materials, affording high performance PSCs. However, non-conjugated small molecule electrolytes for highly efficient PSCs remain rare.

In this work, we designed and synthesized non-conjugated small-molecule organic electrolytes which contain only one zwitterionic unit. Furthermore, a sulfonic group is introduced into the structure to increase the solubility in alcohol, thus facilitating a uniform film formation. The structures of the two interfacial molecules used in this study, 3-(dimethyl(3-sulfopropyl)ammonio)propane-1-sulfonate (DSAPS) and 4-(dimethyl(4-sulfobutyl)ammonio)butane-1-sulfonate (DSABS), are shown in Fig. 1. The PSC active layer is a blend of thieno[3,4-*b*]-thiophene/benzodithiophene (PTB7)[20] as the donor and [6,6]-phenyl C_{71}-butyric acid methyl ester ($PC_{71}BM$) as the acceptor (Fig. 1). Our results demonstrate that incorporating a DSAPS cathode interlayer between the active layer and Al electrode in

[a]*Ningbo Institute of Materials Technology and Engineering, Chinese Academy of Sciences, Ningbo, 315201, China. E-mail: geziyi@nimte.ac.cn*

[b]*University of Chinese Academy of Sciences, Beijing, 100049, China*

[c]*Department of Chemistry and the Materials Research Center, Northwestern University, Evanston, Illinois 60208, USA*

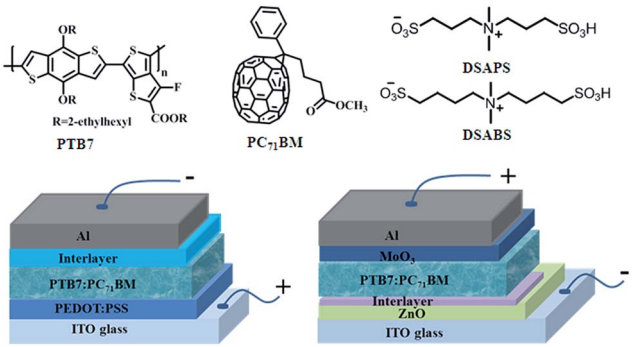

Fig. 1 Molecule structures and schematic of the PSCs device studied in this work (interlayer = none, Ca, LiF, DSAPS or DSABS in conventional devices and none or DSAPS in inverted devices).

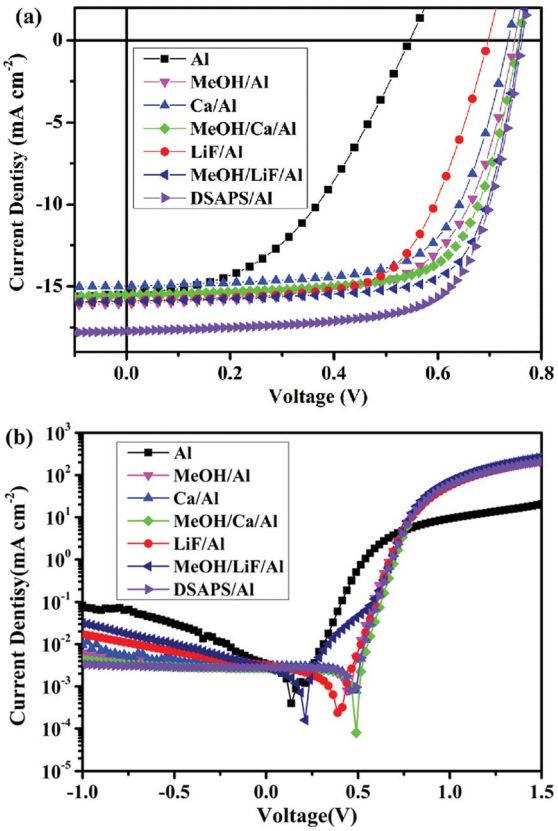

Fig. 2 Current density–voltage (*J*–*V*) characteristics of conventional PTB7:$PC_{71}BM$-based PSCs under (a) AM 1.5G and 100 mW cm^{-2} illumination and (b) in the dark.

conventional PSCs (Fig. 1) dramatically improves the open-circuit voltage (V_{oc}), short-circuit current (J_{sc}) and fill factor (FF) values, resulting in a PCE enhancement from 3.89% to 9.79% (+151% relative enhancement). For inverted PSCs (Fig. 1), the incorporation of DSAPS between the active layer and ZnO layer caused a significant improvement in the J_{sc} and FF values, leading to a PCE from 7.34% to 9.10% (+24% relative enhancement). The methanol treatment has been reported as an efficient approach to improve the performance of PSCs by optimizing the D/A phase separation and removal of the solvent additive or residual solvent in the active layers.[21] Sun *et al.* reported that a combined action of methanol treatment and CPEs can obtain highly efficient PSCs by a two-step strategy.[22] Here, DSAPS dissolves in methanol during a spin-coating process, thus there should be a synergy effect for improving the device efficiency between the methanol treatment and DSAPS interlayer. We discovered that the increase in V_{oc} should be mainly attributed to the methanol treatment, while the DSAPS interlayer primarily enhanced the J_{sc} and FF of PTB7:$PC_{71}BM$-based PSCs. The DSAPS interlayer, as a result of its dipole moment, can also affect the V_{oc} to reduce the WF of electrodes, but its effect is less than the methanol treatment, which is different from the conjugated organic interlayers that can change the V_{oc} of devices.[23,24] The DSAPS interlayer can accelerate the charge extraction and reduce the charge recombination owing to its dipole moment and amine group which may act as the hole traps.[25]

Results and discussion

The conventional device configuration used here, consisting of ITO/PEDOT:PSS/PTB7:$PC_{71}BM$/interlayer/Al (interlayer = none, Ca, LiF, DSAPS, or DSABS), is also shown in Fig. 1. Some of these devices were treated with methanol before device completion and measurements, as described previously.[24] The current density–voltage (*J*–*V*) characteristics of the optimized devices and control devices under AM 1.5G, 100 mW cm^{-2} illumination and in the dark are shown in Fig. 2 and the device parameters are listed in Table 1. Evidently, the devices with DSAPS as the cathode interlayer exhibit the highest PCE of 9.79% compared to the other devices (3.9–8.9%), demonstrating that DSAPS is an effective cathode interfacial modifier. Relative to the control device without an interlayer V_{oc}, J_{sc} and FF of the DSAPS-based devices are dramatically enhanced from 0.55 ± 0.01 V to 0.76 ± 0.01 V, from 15.30 ± 0.16 mA cm^{-2} to 18.20 ± 0.20 mA cm^{-2} and from 45.5% ± 1 to 70.0% ± 1, respectively. The bare Al devices treated with methanol also exhibited an increased V_{oc} (0.76 ± 0.01 V), J_{sc} (15.87 ± 0.11 mA cm^{-2}) and FF (63.9% ± 1), in agreement with the literature,[11a,c] indicating the positive effects of polar solvents on device performance. Interestingly, the V_{oc} of the DSAPS-based devices is similar to that of the methanol-treated ones, but both J_{sc} and FF are larger. J_{sc} and FF correlate to charge-carrier mobilities and the internal field. Hence, the performance improvement due to the dipolar DSAPS zwitterion may result from enhanced charge-carrier mobilities and the internal field, which facilitate the charge transport and extraction, and reduce the bimolecular recombination at the interface.[23] The dark *J*–*V* characteristics in Fig. 2b indicate that the DSAPS-based devices exhibit a better diode rectification and smaller reverse leakage current.[26] The external quantum efficiency (EQE) and the calculated J_{sc} of the devices with a DSAPS layer are also higher compared with the control devices (Fig. S2 and Table S2†). Compared to the control Al devices without methanol treatment, the J_{sc} and FF of the devices containing a Ca or LiF interlayer plus methanol treatment are improved, however the V_{oc} values are basically the same as the devices with

Table 1 Photovoltaic performance of PTB7:$PC_{71}BM$-based PSCs with or without an interlayer and methanol treatment

Interlayer	V_{oc} [V]	J_{sc} [mA cm^{-2}]	FF [%]	PCE[a] [%] avg	PCE [%] best
None	0.55 ± 0.01	15.30 ± 0.16	45.5 ± 1	3.83	3.89
MeOH/Al	0.76 ± 0.01	15.87 ± 0.20	63.9 ± 1	7.70	7.78
Ca/Al	0.73 ± 0.01	14.95 ± 0.21	66.1 ± 1	7.21	7.35
MeOH/Ca/Al	0.76 ± 0.01	15.27 ± 0.19	69.5 ± 1	8.06	8.15
LiF/Al	0.70 ± 0.01	15.75 ± 0.25	64.9 ± 1	7.16	7.34
MeOH/LiF/Al	0.76 ± 0.01	15.85 ± 0.19	72.3 ± 1	8.71	8.89
DSAPS/Al	0.76 ± 0.01	18.20 ± 0.23	70.0 ± 1	9.68	9.79

[a] The average values of 50 devices.

a DSAPS interlayer or only methanol treatment. This result suggests that methanol treatment possibly plays a decisive role in the V_{oc} *via* changing the built-in voltage (V_{bi}) and surface potential of the active layer of PTB7:$PC_{71}BM$-based PSCs.[11c] Nevertheless, the DSAPS interlayer mainly increases the J_{sc} and FF, which is inconsistent with the literature which usually concluded that V_{oc} enhanced from the interlayer.[23,24]

To examine the origin of the difference in V_{oc}, scanning Kelvin probe microscopy (SKPM) was used to provide essential information on the surface potential of the active layer interface. The surface potential difference (SPD) (the average value obtained from a typical area of 500 nm × 500 nm) of the tip and the top film of the active layer with different treatments is shown in Fig. 3. The SPD of the PTB7:$PC_{71}BM$ film with methanol treatment was found to rise by ~0.21 V compared to that of the pristine PTB7:$PC_{71}BM$ film, implying an optimization of the interface composition and reduction of the Schottky barrier at the organic/metal interface, thus leading to a better device performance.[21,22] The SPD of the PTB7:$PC_{71}BM$ film with a DSAPS layer displayed about ~0.18 V improvement relative to that of the pristine PTB7:$PC_{71}BM$ film, which showed that DSAPS could reduce the Schottky barrier and facilitate the charge extraction. Meanwhile, it can be seen that the surface potential of the PTB7:$PC_{71}BM$ film with methanol treatment is more positive than that of the PTB7:$PC_{71}BM$ film with a DSAPS layer, suggesting that methanol treatment plays a greater influence on the V_{oc}. However, the J_{sc} of the DSAPS-based devices is higher than that of the devices with methanol treatment, implying that the interfacial dipole between DSAPS and the Al cathode mainly improves the charge extraction rather than changing the V_{oc}.

To further understand the synergy influence of methanol treatment and the DSAPS interlayer, we fabricated inverted PSCs of structure ITO/ZnO/with or without interlayer/PTB7:$PC_{71}BM$/MoO_x/Al (Fig. 1 and 4). The device performances are collected in Table 2. Interestingly, all devices exhibit a similar V_{oc} of 0.75 V, suggesting that methanol treatment mainly affects the built-in voltage (V_{bi}) and surface potential of

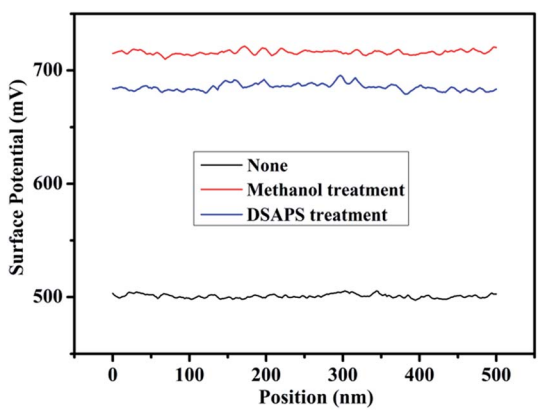

Fig. 3 The surface potential difference of the PTB7:$PC_{71}BM$ films with different treatments.

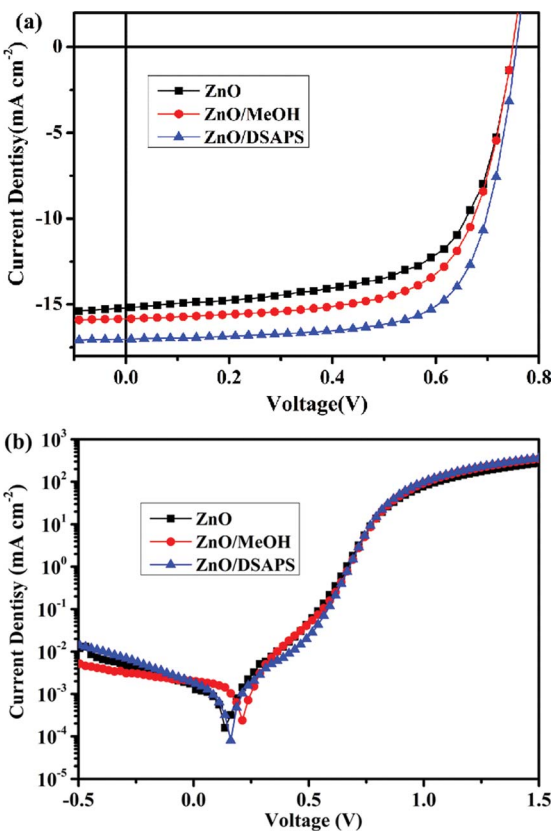

Fig. 4 Current density–voltage (J–V) characteristics of the inverted PSCs under (a) AM 1.5G and 100 mW cm^{-2} illumination and (b) in the dark.

Table 2 Photovoltaic performance of the PTB7:$PC_{71}BM$-based inverted PSCs with or without an interlayer

Interlayer	V_{oc} [V]	J_{sc} [mA cm^{-2}]	FF [%]	PCE[a] [%] avg	PCE [%] best
ZnO	0.75 ± 0.01	15.01 ± 0.18	64.2 ± 1	7.22	7.34
ZnO/MeOH	0.75 ± 0.01	15.83 ± 0.17	66.1 ± 1	7.85	7.94
ZnO/DSAPS	0.75 ± 0.01	17.01 ± 0.21	70.3 ± 1	8.97	9.10

[a] The average values of 50 devices.

the active layer to enhance the V_{oc}. It also implies that even though the DSAPS interlayer could modify the energy level of ZnO, it hardly affected the V_{oc} of the devices. The WF change of the ZnO layer with or without a DSAPS interlayer was investigated by ultraviolet photoelectron spectroscopy (UPS) measurements (Fig. S3†). The WF shifted from 4.41 to 4.31 eV upon ZnO modification with DSAPS, but it did not change the V_{oc} of the ZnO-based devices, which is similar to the literature.[27] Furthermore, the J_{sc} and FF slightly increase from 15.01 ± 0.18 mA cm^{-2} and 64.2 ± 1% (control ZnO) to 15.83 ± 0.17 mA cm^{-2} and 66.1% ± 1 (ZnO/MeOH), respectively, possibly because methanol reduces the surface defect of the ZnO film. The J_{sc} and FF of the DSAPS-based devices strongly increase to 17.01 ± 0.21 mA cm^{-2} and 70.3% ± 1, respectively, illustrating that the DSAPS interlayer can effectively extract the charge and reduce the charge recombination at the interface. Note, the J_{sc} of the inverted devices with a DSAPS interlayer is lower than that of the conventional devices, which may result from the device structure and effect of methanol treatment on the active layer, as well as the better interfacial contact between the DSAPS interlayer and Al electrode than that between the DSAPS interlayer and ZnO.

To gain further insights into the interlayer structural *vs.* processing reasons affecting the device performance, we designed and synthesized the DSABS molecule (Fig. 1) with a longer alkyl chain. Fig. 5 shows the molecular orbital topology of DSAPS and DSABS derived from density functional theory (DFT) computations. The lowest unoccupied molecular orbital (LUMO) centers around the N^+ atom while the highest occupied molecular orbital (HOMO) locates around the SO_3^- group. The LUMO and HOMO energies of DSABS are higher (−1.50 eV and −6.73 eV, respectively) compared to those of DSAPS (−1.23 eV and −6.11 eV, respectively), possibly attributed to the longer electron-donating alkyl chain. The calculated dipole moment of DSAPS is 22.1 D and that of DSABS is 29.5 D. Such large dipole moments can induce considerable interface dipoles when contacted with (semi)conducting materials, lowering the WF.[19] The devices with a DSAPS or DSABS interlayer which are processed from methanol showed a basically consistent V_{oc}, 0.76 V, for the same batch of devices (Table S4 and Fig. S5†). However, it was reasonable to assume that the V_{oc} of the devices with a DSAPS and DSABS interlayer should be different due to their different energy level and degree of dipole moment, which can change the built-in voltage. This result further suggests that the effect of methanol treatment on V_{oc} is much larger than the role of the DSAPS and DSABS interlayer, which ultimately determines the V_{oc} of the conventional devices. The devices with a DSABS or DSAPS interlayer show a similar J_{sc} of 18.26 mA cm^{-2} and 18.42 mA cm^{-2}, and FF of 69.7% and 69.9%, respectively. The PCEs of the devices with DSAPS or DSABS are as high as 9.79% and 9.69%, individually. It also illustrates that non-conjugated DSAPS and DSABS mainly enhance charge extraction and reduce charge recombination at the interface (Fig. 6).

Ultraviolet-visible (UV-vis) absorption spectra of the DSAPS and DSABS films and solutions showed a negligible absorption in the visible light region (Fig. S6†), thus these interlayers do not reduce sunlight transmission. The UV-vis absorption spectra of the PTB7:$PC_{71}BM$ blend films with methanol treatment, a DSAPS interlayer or DSABS interlayer showed little difference compared to the pristine film (Fig. S7†). The surface morphology was investigated by atomic force microscopy (AFM)

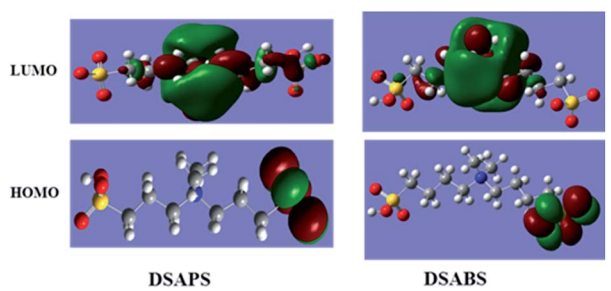

Fig. 5 The graphical electron cloud distribution of DSAPS and DSABS derived from DFT calculations.

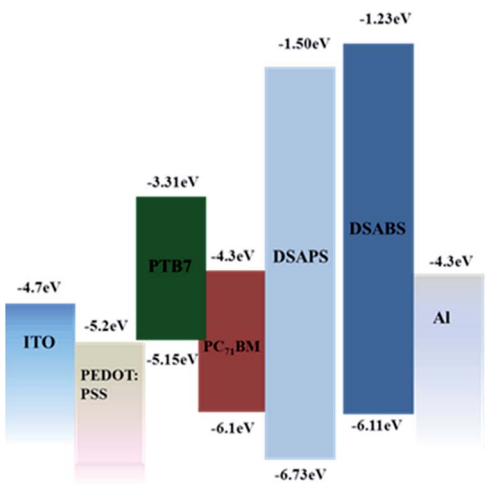

Fig. 6 Energy levels of the PTB7:$PC_{71}BM$-based PSCs.

(Fig. S8†), in which the pristine PTB7:$PC_{71}BM$ film exhibits a surface root mean square (RMS) roughness of 1.65 nm. The methanol-treated film has a similar RMS of 1.67 nm and shows no obvious change in morphology. The PTB7:$PC_{71}BM$/DSAPS or DSABS films are smooth without apparent surface reconstruction, with a RMS roughness of 1.70 nm and 1.75 nm, respectively.

The effects of the DSAPS interlayer on charge transport were studied by the space charge limited current (SCLC) measurements of hole-only and electron-only devices with configurations of ITO/PEDOT:PSS (30 nm)/PTB7:$PC_{71}BM$ (110 nm)/with or without interlayer (5 nm)/MoO_x (5 nm)/Au (100 nm) and ITO/Al (80 nm)/PTB7:$PC_{71}BM$ (110 nm)/with or without interlayer (5 nm)/Al (100 nm), respectively. The *J*–*V* curve (Fig. S9†) was fit using the Mott–Gurney law, $J = 9\varepsilon_r\varepsilon_0\mu V^2/8L^3$, where $\varepsilon_r\varepsilon_0$ is the dielectric permittivity of the active layer, μ is the mobility, V is the effective voltage, and L is the thickness of the active layer.[28] In the PTB7:$PC_{71}BM$/Al control device the hole mobility values are 8.9×10^{-5} cm^2 V^{-1} s^{-1}, while the values of the PTB7:PC_{71}-BM/Methanol treatment/Al and PTB7:$PC_{71}BM$/DSAPS/Al devices are 1.7×10^{-4} cm^2 V^{-1} s^{-1} and 3.2×10^{-4} cm^2 V^{-1} s^{-1}, respectively, which is an increase by an order of magnitude. Simultaneously, the values of electron mobility also improved from 9.8×10^{-4} cm^2 V^{-1} s^{-1} to 1.3×10^{-3} cm^2 V^{-1} s^{-1} and 2.6×10^{-3} cm^2 V^{-1} s^{-1}. It can be seen that the devices with a DSAPS interlayer have a higher and more balanced charge mobility which may increase the J_{sc} and FF in the devices, implying that the DSAPS interlayer can efficiently reduce the charge transport barrier and recombination.

To rationalize the influence of the DSAPS interlayer on the charge recombination, PTB7:$PC_{71}BM$-based devices with and without a DSAPS interlayer were analyzed by an impedance measurement. Fig. 7 shows the Nyquist plots of impedance spectroscopy of the devices in the 1 Hz to 1 MHz frequency range with an oscillation amplitude of 10 mV in the dark without a bias voltage. In Nyquist plots, the diameter of the semicircle represents the shunt resistance (R_{sh}) of the device, which is related to the carrier loss and charge recombination.[29] The largest R_{sh} of the device with a DSAPS interlayer suggests the least charge recombination, which agrees well with the highest J_{sc} and best photovoltaic performance. In addition, series resistance (R_s) can be obtained from the impedance spectroscopy. The calculated R_s of the control device is 7.1 Ω cm^2, while the R_s values of the MeOH-treated and DSAPS devices are reduced to 4.4 Ω cm^2 and 3.5 Ω cm^2, respectively. The device with a DSAPS interlayer possesses the lowest R_s and highest R_{sh} compared to the device with methanol treatment and the control device, demonstrating that the DSAPS interlayer can effectively suppress charge recombination and facilitate the charge extraction at the interface, which is in accord with the observed improvement of J_{sc} and FF.[30]

Finally, to demonstrate the potential application of the DSAPS interlayer larger area device, we prepared PSCs from 4 to 12.47 mm^2, and from small square devices to large circular devices. The principal photovoltaic parameters of these devices are listed in Table S5.† The PCE for the 4 mm^2 device is 9.79%, with a V_{oc} of 0.76 V, J_{sc} of 18.42 mA cm^{-2} and FF of 69.9%. When the active area of the devices extends to 12.57 mm^2, a slightly lower J_{sc} of 17.71 mA cm^{-2} and a similar FF of 69.8% were obtained, leading to a slightly lower PCE of 9.41%, which can be attributed to the increase of the ITO electrode series resistance.[31] Notably, the V_{oc} and FF of PSCs with DSAPS minimally change with increasing device active area, suggesting that the synergy effect of methanol treatment and the DSAPS interlayer on the improvement of the PSCs performance is uniform on a relatively large area, which is beneficial for the large-area fabrication of PSCs.

Additionally, the stability of the devices with the DSAPS interlayer was investigated since the sulfonic group is generally thought to have an adverse impact on the Al electrode.[32] We monitored the device PCE *versus* time in an argon atmosphere glovebox without encapsulation. It is notable that the PCE of the device with the DSAPS interlayer retained >85% of its original PCE value after 30 days storage compared to the control device with a Ca interlayer, which only retained 73% of its original value of PCE (Fig. S11†). The photovoltaic parameters of the device with the DSAPS interlayer all changed to a certain extent with the V_{oc} changing from 0.76 V to 0.77 V, J_{sc} from 17.71 mA cm^{-2} to 16.22 mA cm^{-2} and FF from 69.8% to 67.2%, which still remained relatively high values.

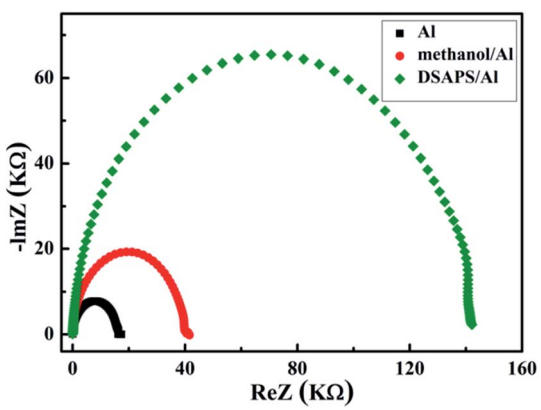

Fig. 7 Impedance spectroscopy of the PTB7:$PC_{71}BM$-based PSCs with or without a DSAPS interlayer.

Conclusions

We have developed a novel non-conjugated sulfonic-ammonium organic small-molecule zwitterion, DSAPS, as an effective cathode interlayer both in conventional and inverted PSCs and obtained a high efficiency of 9.79%. Methanol treatment plays the decisive role in the V_{oc} of PTB7:$PC_{71}BM$-based conventional PSCs. DSAPS can efficiently enhance the charge extraction and reduce charge recombination owing to its dipole moment. This synergy effect of methanol treatment and the DSAPS interlayer can effectively improve the device performance of PTB7:PC_{71}-BM-based PSCs by simple and eco-friendly spin-coating fabrication. It is worth noting that the low-cost sulfonic DSAPS not only efficiently improves the device performance, but also increases the stability of the PTB7:$PC_{71}BM$-based conventional

PSCs. Our findings reveal new strategies to design simple non-conjugated organic small-molecule electrolytes for highly efficient PSCs.

Experimental

Materials

PTB7, $PC_{71}BM$ and 1,8-diiodooctane (DIO) were purchased from 1-Material, American Dye Source, Inc. and Acros, respectively and used as received. The ITO glasses (1.2 mm thick, ≤15 Ω per square, transmittance > 90%) were purchased from the Nippon Sheet Glass Company, Ltd, and cleaned sequentially with deionized water, ethanol, acetone and isopropanol for 40 min each, then treated with UV-ozone for 20 min. PEDOT:PSS was purchased from the Baytron Company.

Device fabrication

The device structure was ITO/PEDOT:PSS (Baytron® P VP Al 4083)/PTB7:$PC_{71}BM$/with or without interlayer/Al. The PEDOT:PSS aqueous solution was filtered through a 0.45 μm filter and spin-coated at 4000 rpm for 1 min onto the treated ITO substrate and annealed at 140 °C for 10 min. Then the active layer, about 110 nm, was spin-cast from a solution with a PTB7:$PC_{71}BM$ ratio of 1 : 1.5 by weight (PTB7 concentration of 10 mg mL^{-1}) in a chlorobenzene/1,8-diiodooctane (97 : 3 vol%) mixed solvent at 2000 rpm for 2 min and put in a vacuum for 30 min. The interlayer materials were dissolved in methanol in the presence of a small amount of acetic acid (99 : 1 vol%) and their solutions (1.5 mg mL^{-1}) were spin-coated onto the active layer and put in a vacuum for 30 min. The thickness was controlled by the concentration of the solution and the spin speed, from 1000 rpm to 6000 rpm. The Al electrode (100 nm) was evaporated in a vacuum chamber (3×10^{-6} mbar) through a shadow mask to define the active area of the devices (4 or 12.57 mm^2). ZnO was prepared according to the literature.[33] MoO_x (10 nm) was evaporated in a vacuum chamber (3×10^{-6} mbar) through a shadow mask.

Characterization and measurement

Current density–voltage (*J*–*V*) characteristics of the devices were measured under simulated solar light (100 mW cm^{-2}; AM 1.5G) provided by a Newport-Oriel® Sol3A 450 W solar simulator and the devices were stored in an Ar atmosphere without encapsulation. The device parameters were recorded with a Keithley 2440 Source Measure Unit. The intensity of the simulated solar light was calibrated by a standard Si photodiode detector (PV measurements Inc.), which was calibrated at the National Renewable Energy Laboratory (NREL). The external quantum efficiency (EQE) spectra were determined using a Newport-Oriel® IQE 200™ which was calibrated by a standard Si/Ge solar cell under illumination with monochromatic light from a Xe lamp at room temperature in air. The thickness of the films was determined using a surface profiler (Dektak 150).

^1H and ^{13}C NMR spectra were collected with a Bruker DMX-400 Spectrometer. The UV-vis absorption spectra were measured by a Perkin-Elmer Lambda 950 spectrophotometer. The surface images and roughness were conducted on a Veeco Dimension 3100V atomic force microscope. Mass spectra were measured by an XEVO Wafer high-performance liquid chromatography and mass spectrometer. Impedance spectra were obtained by a ZENNIUM of the Zahner Company. The DFT calculations were performed with the Gaussian09 series of programs using the B3LYP hybrid functional and 6-31G(d) basis set. Ultraviolet photoelectron spectroscopy (UPS) measurements were obtained by a Kratos ULTRADLD UPS/XPS system (Kratos analytical, Manchester, U.K.) with He I radiation at 21.2 eV from a discharge lamp operated at 20 mA, a pass energy of 5 eV, and a channel width of 25 meV.

Acknowledgements

This work was financially supported from the National Natural Science Foundation of China (21574144, 51273209, 51411140244), the High-end Foreign Expert of State Administration of Foreign Experts Affairs, Zhejiang Provincial Natural Science Foundation of China (LR16B040002), Ningbo Municipal Science and Technology Innovative Research Team (2015B11002), State Key Laboratory of Luminescence and Applications, and State Key Laboratory of Polymer Physics and Chemistry, Changchun Institute of Applied Chemistry, CAS, and CAS Interdisciplinary Innovation Team.

Notes and references

1 (*a*) C. R. McNeill and N. C. Greenham, *Adv. Mater.*, 2009, **21**, 3840; (*b*) M. A. Green, K. Emery, Y. Hishikawa and W. Warta, *Prog. Photovoltaics*, 2011, **19**, 84; (*c*) Y. F. Li, *Acc. Chem. Res.*, 2012, **45**, 723.

2 J.-D. Chen, C. H. Cui, Y.-Q. Li, L. Zhou, Q.-D. Ou, C. Li, Y. F. Li and J.-X. Tang, *Adv. Mater.*, 2015, **27**, 1035.

3 Y. Liu, J. Zhao, Z. Li, C. Mu, W. Ma, H. Hu, K. Jiang, H. Lin, H. Ade and H. Yan, *Nat. Commun.*, 2013, **4**, 1446.

4 Z. C. He, B. Xiao, F. Liu, H. B. Wu, Y. Yang, S. Xiao, C. Wang, T. P. Russell and Y. Cao, *Nat. Photonics*, 2015, **9**, 174.

5 S. Braun, W. R. Salaneck and M. Fahlman, *Adv. Mater.*, 2009, **21**, 1450.

6 H. Choi, J. S. Park, E. Jeong, G.-H. Kim, B. R. Lee, S. O. Kim, M. H. Song, H. Y. Woo and J. Y. Kim, *Adv. Mater.*, 2011, **23**, 2759.

7 J. H. Seo, E. B. Namdas, A. Gutacker, A. J. Heeger and G. C. Bazan, *Appl. Phys. Lett.*, 2010, **97**, 043303.

8 Y. H. Zhou, C. Fuentes-Hernandez, J. Shim, J. Meyer, A. J. Giordano, H. Li, P. Winget, T. Papadopoulos, H. Cheun, J. Kim, M. Fenoll, A. Dindar, W. Haske, E. Najafabadi, T. M. Khan, H. Sojoudi, S. Barlow, S. Graham, J.-L. Brédas, S. R. Marder, A. Kahn and B. Kippelen, *Science*, 2012, **336**, 327.

9 S. H. Park, A. Roy, S. Beaupré, S. Cho, N. Coates, J. S. Moon, D. Moses, M. Leclerc, K. Lee and A. J. Heeger, *Nat. Photonics*, 2009, **3**, 297.

10 (*a*) C. J. Brabec, S. E. Shaheen, C. Winder and N. S. Sariciftci, *Appl. Phys. Lett.*, 2002, **80**, 1288; (*b*) J. Wang, F. Zhang, L. Li, Q. An, J. Zhang, W. Tang and F. Teng, *Sol. Energy Mater. Sol.*

Cells, 2014, **130**, 15; (*c*) P. Peumans, A. Yakimov and S. R. Forrest, *J. Appl. Phys.*, 2003, **93**, 3693; (*d*) G. Li, C.-W. Chu, V. Shrotriya, J. Huang and Y. Yang, *Appl. Phys. Lett.*, 2006, **88**, 253503; (*e*) M. S. White, D. C. Olson, S. E. Shaheen, N. Kopidakis and D. S. Ginley, *Appl. Phys. Lett.*, 2006, **89**, 143517; (*f*) D. W. Zhao, P. Liu, X. W. Sun, S. T. Tan, L. Ke and A. K. K. Kyaw, *Appl. Phys. Lett.*, 2006, **95**, 153304; (*g*) J. H. Lee, S. Cho, A. Roy, H.-T. Jung and A. J. Heeger, *Appl. Phys. Lett.*, 2010, **96**, 163303; (*h*) H.-L. Yip, S. K. Hau, N. S. Baek, H. Ma and A. K.-Y. Jen, *Adv. Mater.*, 2008, **20**, 2376; (*i*) M. D. Irwln, D. B. Buchholz, A. W. Halns, R. P. H. Chang and T. J. Marks, *Proc. Natl. Acad. Sci. U. S. A.*, 2008, **105**, 2783.

11 (*a*) J. H. Seo, A. Gutacker, Y. M. Sun, H. B. Wu, F. Huang, Y. Cao, U. Scherf, A. J. Heeger and G. C. Bazan, *J. Am. Chem. Soc.*, 2011, **133**, 8416; (*b*) S. Nam, J. Jang, H. Cha, J. Hwang, T. K. An, S. Park and C. E. Park, *J. Mater. Chem.*, 2012, **22**, 5543; (*c*) H. Q. Zhou, Y. Zhang, J. Seifter, S. D. Collins, C. Luo, G. C. Bazan, T.-Q. Nguyen and A. J. Heeger, *Adv. Mater.*, 2013, **25**, 1646; (*d*) Z.-K. Tan, Y. Vaynzof, D. Credgington, C. Li, M. T. L. Casford, A. Sepe, S. Huettner, M. Nikolka, F. Paulus, L. Yang, H. Sirringhaus, N. C. Greenham and R. H. Friend, *Adv. Funct. Mater.*, 2014, **24**, 3051; (*e*) Y. Wang, Y. Liu, S. Chen, R. Peng and Z. Ge, *Chem. Mater.*, 2013, **25**, 3196.

12 (*a*) S.-S. Kim, S.-I. Na, J. Jo, D.-Y. Kim and Y.-C. Nah, *Appl. Phys. Lett.*, 2008, **93**, 073307; (*b*) H. A. Atwater and A. Polman, *Nat. Mater.*, 2010, **9**, 205.

13 X. He, F. Gao, G. Tu, D. Hasko, S. Hüttner, U. Steiner, N. C. Greenham, R. H. Friend and W. T. S. Huck, *Nano Lett.*, 2010, **10**, 1302.

14 (*a*) Z. He, C. Zhong, S. Su, M. Xu, H. Wu and Y. Cao, *Nat. Photonics*, 2012, **6**, 591; (*b*) Y. Liu, Z. A. Page, T. P. Russell and T. Emrick, *Angew. Chem., Int. Ed.*, 2015, **54**, 11485.

15 (*a*) K. Yao, M. Salvador, C. Chueh, X. Xin, Y. Xu, W. Dane, T. Hu, Y. Chen, D. S. Ginger and A. K. Jen, *Adv. Energy Mater.*, 2014, **4**, 1400206; (*b*) W. Zhang, Y. Wu, Q. Bao, F. Gao and J. Fang, *Adv. Energy Mater.*, 2014, **4**, 1400359; (*c*) C. Duan, C. Zhong, C. Liu, F. Huang and Y. Cao, *Chem. Mater.*, 2012, **24**, 1682.

16 C. Duan, K. Zhang, C. Zhong, F. Huang and Y. Cao, *Chem. Soc. Rev.*, 2013, **42**, 9071.

17 X. H. Ouyang, R. Peng, L. Ai, X. Zhang and Z. Ge, *Nat. Photonics*, 2015, **9**, 520.

18 F. L. Zhang, M. Ceder and O. Inganäs, *Adv. Mater.*, 2007, **19**, 1835.

19 H. Lee, E. Puodziukynaite, Y. Zhang, J. C. Stephenson, L. J. Richter, D. A. Fischer, D. M. DeLongchamp and T. Emrick, *J. Am. Chem. Soc.*, 2015, **137**, 540.

20 Y. Liang, Z. Xu, J. B. Xia, S.-T. Tsai, Y. Wu, G. Li, C. Ray and L. Yu, *Adv. Mater.*, 2010, **22**, E135.

21 (*a*) S. Nam, J. Jang, H. Cha, J. Hwang, T. K. An, S. Park and C. E. Park, *J. Mater. Chem.*, 2012, **22**, 5543; (*b*) L. Ye, Y. Jing, X. Guo, H. Sun, S. Zhang, M. Zhang, L. Huo and J. Hou, *J. Phys. Chem. C*, 2013, **117**, 14920.

22 Q. Sun, F. Zhang, J. Wang, Q. An, C. Zhao, L. Li, F. Teng and B. Hu, *J. Mater. Chem. A*, 2015, **3**, 18432.

23 Z. He, C. Zhong, X. Huang, W.-Y. Wong, H. Wu, L. Chen, S. Su and Y. Cao, *Adv. Mater.*, 2011, **23**, 4636.

24 M. Lv, S. Li, J. J. Jasieniak, J. Hou, J. Zhu, Z. Tan, S. E. Watkins, Y. Li and X. Chen, *Adv. Mater.*, 2013, **25**, 6889.

25 C. Duan, W. Cai, B. B. Y. Hsu, C. Zhong, K. Zhang, C. Liu, Z. Hu, F. Huang, G. C. Bazan, A. J. Heeger and Y. Cao, *Energy Environ. Sci.*, 2013, **6**, 3022.

26 D. Bilby, B. Frieberg, S. Kramadhati, P. Green and J. Kim, *ACS Appl. Mater. Interfaces*, 2014, **6**, 14964.

27 K. Zhang, C. Zhong, S. Liu, C. Mu, Z. Li, H. Yan, F. Huang and Y. Cao, *ACS Appl. Mater. Interfaces*, 2014, **6**, 10429.

28 P. W. M. Blom and M. C. J. M. Vissenberg, *Mater. Sci. Eng., R*, 2000, **27**, 53.

29 (*a*) B. J. Leever, C. A. Bailey, T. J. Marks, M. C. Hersam and M. F. Durstock, *Adv. Energy Mater.*, 2012, **2**, 120; (*b*) H. Li, J. Cao, Q. Zhou, L. Ding and J. Wang, *Nano Energy*, 2015, **15**, 125.

30 T. Kuwabara, Y. Kawahara, T. Yamaguchi and K. Takahashi, *ACS Appl. Mater. Interfaces*, 2009, **1**, 2107.

31 C. Cui, X. Guo, J. Min, B. Guo, X. Cheng, M. Zhang, C. J. Brabec and Y. Li, *Adv. Mater.*, 2015, **27**, 7469.

32 (*a*) M. Jørgensen, K. Norrman and F. C. Krebs, *Sol. Energy Mater. Sol. Cells*, 2008, **92**, 686; (*b*) C. K. Song, A. C. White, L. Zeng, B. J. Leever, M. D. Clark, J. D. Emery, S. J. Lou, A. Timalsina, L. X. Chen, M. J. Bedzyk and T. J. Marks, *ACS Appl. Mater. Interfaces*, 2013, **5**, 9224.

33 S.-H. Liao, H.-J. Jhuo, Y.-S. Cheng and S.-A. Chen, *Adv. Mater.*, 2013, **25**, 4766.